Photon Bloch Oscillations in Porous Silicon Optical Superlattices

V. Agarwal
Centro de Investigacion en Ingenieria y Ciencias Applicadas UAEM, Avenida Universidad 1001, Colonia Chamilpa, CP 62210, Cuernavaca, Morelos, Mexico

J. A. del Río
Centro de Investigación en Energía, Universidad Nacional Autónoma de México, Temixco 62580, Morelos, Mexico

G. Malpuech, M. Zamfirescu, and A. Kavokin
LASMEA, CNRS/Université Clermont-Ferrand II, Blaise Pascal, 24 Avenue des Landais, 63177 Aubière CEDEX, France

D. Coquillat, D. Scalbert, M. Vladimirova, and B. Gil
GES, CNRS/Université Montpellier II, 34095 Montpellier CEDEX 5, France
(Received 1 July 2003; published 2 March 2004)

We report the first observation of oscillations of the electromagnetic field in an optical superlattice based on porous silicon. These oscillations are an optical equivalent of well-known electronic Bloch oscillations in crystals. Elementary cells of our structure are composed by microcavities whose coupling gives rise to the extended collective modes forming optical minigaps and minibands. By varying thicknesses of the cavities along the structure axis, we have created an effective electric field for photons. A very high quality factor of the confined optical state of the Wannier-Stark ladder may allow lasing in porous silicon-based superlattices.

DOI: 10.1103/PhysRevLett.92.097401 PACS numbers: 78.67.Pt, 42.70.Qs, 78.47.+p

Only recently, electronic Bloch oscillations (EBO), i.e., oscillations of an electron within a Brillouin zone induced by an applied electric field [1], have been experimentally demonstrated in semiconductor superlattices [2,3]. An electron in a crystal experiences EBO if its dephasing time because of Zener tunneling or scattering on defects is longer than the oscillation period h/eFd, where e is the elementary charge, F is the applied electric field, and d is the lattice period. Until now, EBO have been observed only in semiconductor superlattices, since these structures have large enough supercells in real space to make a period of the EBO smaller than the dephasing time [4]. Bloch oscillations are expected to be more easily observed in photonic systems, where dephasing processes are less effective. An electric field has no effect on photons so that in optical superlattices a potential gradient should be introduced by other means to observe the photonic Bloch oscillations (PBO). Several optical systems have been proposed [5–10] and studied [11–14] to reveal formation of the photonic Wannier-Stark ladder (PWSL) and PBO. Gradual variation of the photonic band edges has been achieved by variation of photonic crystal cell size along the structure axis. The first experimental observation of a PWSL has been done on a linearly chirped Moiré grating embedded in the core of an optical fiber [11,14]. PBO have also been observed in experiments on two-dimensional waveguide arrays using a linear variation of refractive index superimposed on an unchirped Bragg grating [12,13]. The optical gratings that have been used in these works can be formally considered as optical superlattices. The layers of the lower index material play the role of quantum wells (QWs), and the layers of the higher index are equivalent to the barriers. However, in periodic planar multilayer structures, the interfaces are semitransparent for light, and discrete confined photonic levels cannot be formed in contrast to the electronic multiple QW structures.

Thus, even though the Bragg mirrors exhibit stop bands similar to the minigaps of electronic superlattices, this similarity is not complete. In fact, the real optical equivalent of multiple QWs is microcavities, which are characterized by a discrete spectrum of confined states. Recently, coupled microcavity structures have been investigated theoretically and experimentally [9,15,16]. The optical coupling lifts the degeneracy between optical modes in identical cavities. In the limit of an infinite multiple-microcavity structure, optical bands are formed that are completely analogous to the minibands in semiconductor superlattices. This effect has been evidenced in a two cavity structure based on GaAs [15], whereas the coupling of ten porous silicon-based microcavities has been reported [16]. The great advantage of porous silicon is that it allows the fabrication of very thick multilayer structures [17]. The refractive index of porous silicon is strongly dependent on the degree of its porosity. In case of electrochemical etching of silicon with HF, the porosity is a linear function of the current density for a specific HF concentration and anodization time [18,19]. This opens the way toward growing optical superlattices containing a large number of supercells.

In this Letter, we report the fabrication of two porous silicon optical superlattices containing 20 and 30 microcavities. In order to incline the optical band and obtain PBO, we made the cavity width to linearly increase from the beginning to the end of the structure [9]. Reflection spectra recorded on these two samples show equally spaced reflection dips superimposed on a 1 eV-wide stop band. These dips are a clear signature of formation of a PWSL.

Figure 1 shows the cross-sectional scanning electron microscopy (SEM) image of the sample with 20 microcavities. The image shows five of the coupled microcavities with their respective mirrors. High and low porosity regions of the mirrors are observed as dark and light regions, respectively. The two samples are formed by 20 and 30 λ cavities of refractive index n_A. In the absence of coupling, the energy of the fundamental mode of the ith cavity is E_i, which corresponds to the wavelength in the vacuum $\lambda_i = hc/E_i$. Each cavity is surrounded by two distributed Bragg mirrors (DBRs) built with alternating layers of n_A and n_B ($n_B > n_A$). Thus, each elementary cell of our optical superlattice consists of one DBR containing $2 + 1/2$ pairs of dielectric layers and a λ cavity. The length of each cell is given by

$$d_i = \lambda_i\left(\frac{3/2}{n_A} + \frac{3/4}{n_B}\right). \tag{1}$$

In analogy with the electronic case discussed above, the effective local electric field in each cavity can be defined as

$$F_i = \frac{E_i - E_{i-1}}{ed_i}. \tag{2}$$

Moreover, the eigenmode of the ith cavity can be interpreted as the ith step of the PWSL. In order to obtain PBO, the spacing Δ between the steps of the PWSL must be constant; this implies that $eF_i d_i = \Delta$ for any $i = 1, 2, \ldots, 20$ or 30, or, equivalently,

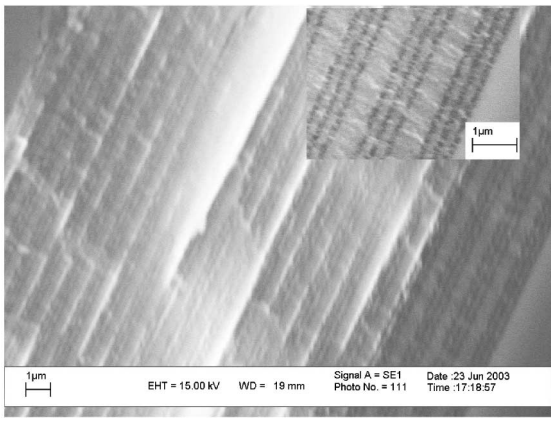

FIG. 1. Cross-sectional SEM image of the 20-cavity sample. The inset shows the amplified view of the structure.

$$\frac{1}{\lambda_i} - \frac{1}{\lambda_{i-1}} = -\frac{\Delta}{hc}, \tag{3}$$

which gives

$$\lambda_i = \frac{\lambda_1}{1 - (i-1)\delta\lambda_1/hc}. \tag{4}$$

The parameters chosen for the 20-cavity samples are $\lambda_1 = 785$ nm and $\Delta = 26$ meV, which corresponds to a PBO period $\tau_B = h/\Delta = 170$ fs. For the 30-cavity samples, they are $\lambda_1 = 785$, $\Delta = 22$ meV, which corresponds to $\tau_B = 200$ fs. The samples have been prepared by the wet electrochemical anodization technique, as described in detail in Ref. [17]. Highly boron-doped silicon substrate ($p++$, 0.001–0.005 Ω cm; $\langle 100\rangle$ orientation) was etched with the electrolyte composed of HF (48%), ethanol (98%), and glycerol (98%) in the volume ratio of 3:7:1. High (70%) and low (45%) porosities were achieved by passing 45 and 5 mA/cm^2 current densities, respectively. The porosity achieved corresponds to $n_A = 1.45$ and $n_B = 1.95$ at the wavelength λ_1. The 20- and 30-cavity samples presented here contain 125 and 185 layers, whereas we have fabricated and reported multilayer structures containing more than 400 layers (Ref. [17]). Further details on the sample preparation will be given elsewhere.

Figure 2(a) shows the experimental and calculated reflection spectrum of the 20-cavity sample. The theoretical reflection spectrum has been calculated by solving linear Maxwell equations using the transfer matrix technique [20]. The allowed miniband energies in the ith cavity are given by the condition [8,9](which is a consequence of the Bloch theorem)

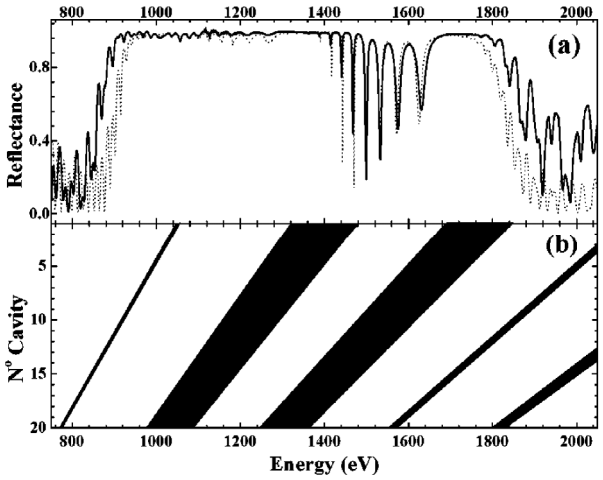

FIG. 2. (a) Solid line: Reflectivity of the 20-cavity sample measured at the incidence angle of 6°. The spectra above and below 1100 meV have been recorded with two different detectors. The dashed line shows the calculated reflectivity of this sample. (b) Band structure of the 20-cavity sample calculated by Eq. (5). White areas represent the allowed minibands and black areas represent the minigaps.

$$-1 \leq [a_{11}(i) + a_{22}(i)]/2 \leq 1, \quad (5)$$

where $a_{11}(i)$ and $a_{22}(i)$ are the diagonal elements of the transfer matrix across the ith period of the structure. This allows us to determine the complete band structure of the sample as it is shown in Fig. 2(b). The lower edge of the first minigap varies between 950 and 1290 meV. In this region, the reflectivity is close to unity but the spectrum exhibits dips whose spacing increases with energy. These dips are due to the interferences taking place between the inclined band and the sample surface. The spacing increases with energy because the thickness of the cavity formed decreases while energy increases. These modes are wide because of the weak reflection coefficient of the air-sample interface. The region between 1330 and 1450 meV shows five sharp reflection dips spaced by 24 meV on the top of a quasiperfect plateau. These dips are due to the coupling of the confined Wannier-Stark states to the outside by light tunneling across the lowest minigap. The better the confinement, the sharper and smaller are the dips. Above 1500 meV, we observe four dips due to interferences between the bottom of the second minigap and the sample surface. The plateau above 1700 meV is due to the complete reflection of light by the second minigap. Note that the spectral features correspond remarkably to the calculated sample band structure.

Figure 3(a) shows the propagation of a 50 fs light pulse within the multicavity structure. The electric field created in the system by an incident pulse of spectral function $g(\omega)$ is calculated by means of the scattering state method [20]. By this formalism, the time- and coordinate-dependent electric field within the structure can be found as follows:

$$E_g(z, t) = \frac{1}{2\pi} \int_{-\infty}^{+\infty} \tilde{E}(\omega, z) g(\omega) \exp(-i\omega t)\, d\omega, \quad (6)$$

where $\tilde{E}(\omega, z)$ are the scattering states of the system [shown in Fig. 3(b)], i.e., the solutions of stationary Maxwell equations which are obtained by the transfer matrix method. At short times, one can observe the tunneling of the incident pulse through the forbidden band. During this first stage, most of the light is reflected by the surface of the sample while only a small percentage enters inside the structure. This light then starts to

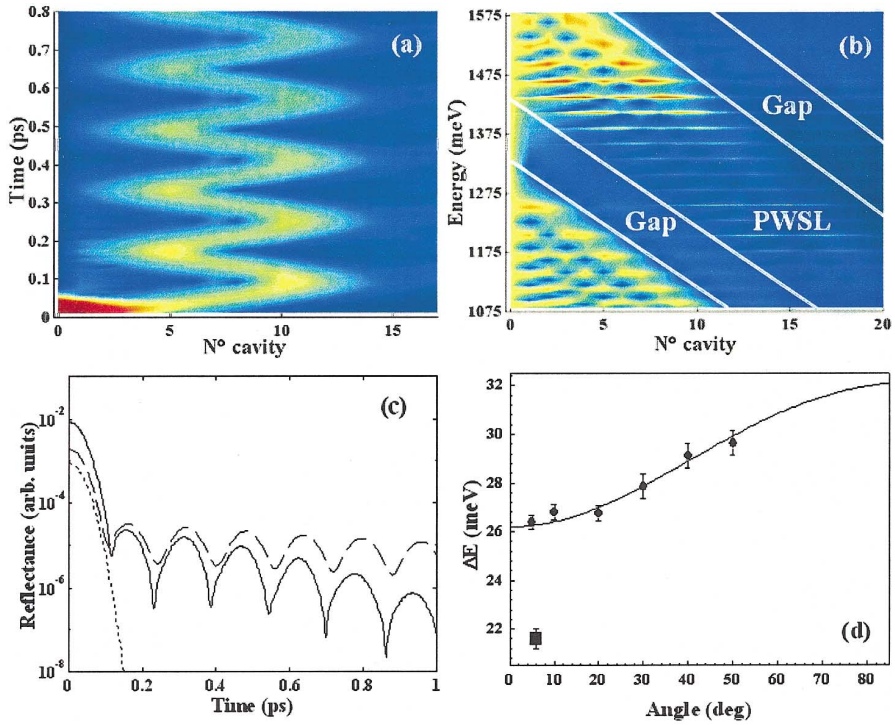

FIG. 3 (color online). (a) Propagation of a 50 fs long light pulse within the 20-cavity sample: Light intensity is shown versus time and space. Bloch oscillations in time domain are clearly seen. (b) Scattering states of the 20-cavity sample. A change from blue to red color (or from dark to bright if the figure appears black and white) corresponds to the increase of the intensity of light. White lines are guides for the eyes. One can observe the formation of the PWSL confined between two minigaps. The states observable in reflection are the broad ones around 1400 meV which are weakly coupled to the outside. Completely confined modes, at lower energy, have very high quality factors. They might allow the occurrence of lasing effect. (c) Solid line: time-resolved reflection of the 20-cavity sample obtained from the measured reflection spectra by formula (7). The dashed line shows the theoretical time-resolved reflection. The dotted line shows the incident light pulse we assumed. (d) Spacing between the states of the PWSL versus excitation angle for the 20-cavity sample (circles) and the 30-cavity sample (squares). The solid line is calculated from Eq. (9) for the 20-cavity sample.

oscillate within the inclined allowed miniband with a regular period of 170 fs. These are PBO which represent the time-domain counterpart of the PWSL. These time-domain oscillations can be detected by measuring the time-resolved reflection of the sample. In the linear regime, and if the background signal is much larger than the dips, the amplitude of the time-resolved reflection can simply be calculated using the experimental cw reflection spectra [21]:

$$r(t) \propto \int_{-\infty}^{+\infty} g(\omega) R(\omega) e^{-i\omega t}\, d\omega, \tag{7}$$

where $R(\omega)$ is the measured reflectivity. Expression (7) is valid only for times longer than the duration of the incident pulse. $r(t)$ can be calculated theoretically as

$$r(t) = \frac{1}{2\pi} \int_{-\infty}^{+\infty} g(\omega) r(\omega) e^{-i\omega t}\, d\omega, \tag{8}$$

where $r(\omega)$ is the amplitude reflection coefficient of the sample. Figure 3(c) shows the experimental and theoretical time-resolved reflection of the sample calculated using (7) and (8), respectively. The incident light pulse is 50 fs long. It is centered on 1400 meV and has a Gaussian shape. One can observe regular oscillations having a period of 170 fs. These oscillations are observable because of the tunneling of photons through the lower inclined gap. There are two ways to modify the period of PBO: by changing the excitation angle or growing another sample with a different thickness gradient. Figure 3(d) shows the spacing between the states of the ladder versus the incidence angle for the 20-cavity sample together with the spacing achieved at quasinormal incidence for the 30-cavity sample. The measured angular dependence of Δ is compared with the theoretical one which is given by

$$\Delta(\theta) = \Delta(0) \frac{\sin^2\theta}{n_a^2} \sqrt{1 - \frac{\sin^2\theta}{n_a^2}}, \tag{9}$$

where θ is the excitation angle. An important feature of these multimicrocavity systems can be seen in Fig. 3(b). The PWSL is formed in a very wide energy range. It is composed of confined optical modes. We are only able to observe modes weakly coupled to the outside while the greatest part of the modes is invisible. Confined photonic modes are characterized by an extremely high quality factor (up to 2000). We believe that the very high quality of the optical confinement here achieved, combined with the emitting properties of porous silicon, could allow one to achieve a lasing effect in porous silicon or in silicon nanocrystals as proposed by Pavesi [22]. One should however note that, in addition to a good photonic confinement, an important requirement to achieve lasing is a high density of light emitting states.

In conclusion, we have exploited the high potentiality of porous silicon for photonic applications [16,17] and demonstrated the appearance of PBO in porous silicon microcavity superlattices. These superlattices are very easy to prepare. Their optical response can be tuned by selecting appropriate etching parameters. We have shown that the period of PBO can be efficiently controlled by tuning the growth parameters. Multiple graded microcavity structures are promising toward a realization of a first laser based on the porous silicon.

We thank Aldo Di Carlo for fruitful discussions and José Campos for technical help. The Mexican groups acknowledge the support of DGAPA-UNAM 117802 and PROMEP, and the French groups the support by both the ACI "Polariton" and the "Equipe projet Polariton" grants.

[1] G. H. Wannier, Phys. Rev. **100**, 1227 (1955); Phys. Rev. **101**, 1835 (1956); Phys. Rev. **117**, 432 (1960); Rev. Mod. Phys. **34**, 645 (1962).
[2] K. Leo, Semicond. Sci. Technol. **13**, 249 (1998).
[3] C. Waschke *et al.*, Phys. Rev. Lett. **70**, 3319 (1993); T. Dekorsky *et al.*, Phys. Rev. B **51**, R17 275 (1995).
[4] G. Nenciu, Rev. Mod. Phys. **63**, 91 (1991); F. Rossi, A. Di Carlo, and P. Lugli, Phys. Rev. Lett. **80**, 3348 (1998); A. Sibille, J. F. Palmier, and F. Laruelle, Phys. Rev. Lett. **80**, 4506 (1998).
[5] G. Monsivais, M. del Castillo-Mussot, and F. Claro, Phys. Rev. Lett. **64**, 1433 (1990).
[6] U. Peschel, T. Persch, and F. Lederer, Opt. Lett. **23**, 1701 (1998).
[7] G. Lenz, I. Talanina, and C. Martijn de Sterke, Phys. Rev. Lett. **83**, 963 (1999).
[8] A. Kavokin, G. Malpuech, A. Di Carlo, P. Lugli, and F. Rossi, Phys. Rev. B **61**, 4413 (2000).
[9] G. Malpuech, A. Kavokin, G. Panzarini, and A. Di Carlo, Phys. Rev. B **63**, 035108 (2001).
[10] P. B. Wilkinson, Phys. Rev. E **65**, 056616 (2002).
[11] C. Martijn de Sterke *et al.*, Phys. Rev. E **57**, 2365 (1998).
[12] T. Persch *et al.*, Phys. Rev. Lett. **83**, 4752 (1999).
[13] R. Morandotti *et al.*, Phys. Rev. Lett. **83**, 4756 (1999).
[14] I. Talanina and C. Martijn de Sterke, Phys. Rev. A **63**, 053802 (2001).
[15] G. Panzarini *et al.*, Phys. Rev. B **59**, 5082 (1999).
[16] M. Ghullinyan, C. J. Oton, Z. Gaburro, P. Bettotti, and L. Pavesi, Appl. Phys. Lett. **82**, 1550 (2003).
[17] V. Agarwal and J. A. del Rio, Appl. Phys. Lett. **82**, 1512 (2003).
[18] V. Agarwal, R. Mehra, and P. C. Mathur, Thin Solid Films **358**, 196 (2000); L. Pavesi, La Revista del Nuevo Cimento **20**, 18 (1997).
[19] J. E. Lugo, J. A. del Río, and J. Tagüeña. J. Appl. Phys. **81**, 1923 (1997); W. Theiss and S. Hilbrich, *Properties of Porous Silicon*, edited by L. T. Canham, EMIS Data Reviews Series (INSPEC/IEE, London, 1998), p. 223.
[20] G. Malpuech and A. Kavokin, Semicond. Sci. Technol. **16**, R1 (2001).
[21] G. Malpuech, A. Kavokin, J. Leymarie, and A. Vasson, Solid State Commun. **113**, 185 (2000); M. Zamfirescu *et al.*, Phys. Rev. B **64**, 121304(R) (2002).
[22] L. Pavesi, L. Dal Negro, C. Mazzoleni, G. Franzo, and F. Priolo, Nature (London) **408**, 440 (2000).